



# Lamina Cribrosa Morphology in Glaucomatous Eyes with Hemifield Defect in a Korean Population

Ji-Ah Kim, MD,<sup>1</sup> Tae-Woo Kim, MD,<sup>1</sup> Eun Ji Lee, MD,<sup>1</sup> Michaël J.A. Girard, PhD,<sup>2,3</sup> Jean Martial Mari, PhD<sup>4</sup>

**Purpose:** To compare regional variations in lamina cribrosa (LC) curvature and depth between healthy eyes (group 1) and naïve eyes with primary open-angle glaucoma (POAG) having superior (group 2), inferior (group 3), and both (group 4) hemifield retinal nerve fiber layer (RNFL) defects.

**Design:** Cross-sectional study.

**Participants:** Each group consisted of 39 eyes of 39 Korean patients who were matched for age, sex, and axial length.

**Methods:** The LC curvature index (LCCI) and LC depth (LCD) were measured in B-scan images obtained using enhanced depth imaging OCT at 7 locations spaced equidistantly across the vertical optic disc diameter. Superior and inferior LCCI and LCD were compared by calculating the superior-to-inferior (Sup/Inf) ratios.

**Main Outcome Measures:** Comparisons of LCCI, LCD, and Sup/Inf ratio among the 4 groups.

**Results:** Compared with healthy eyes (group 1), LCCIs were larger at the superior and middle planes in group 2, at the inferior and middle planes in group 3, and at all planes in group 4 ( $P \leq 0.003$ ). The LCD showed similar results, but there was no difference in superior planes between groups 1 and 2. The Sup/Inf ratio of LCCI differed significantly between groups 1 (1.03) and 2 (1.20), groups 1 and 3 (0.79), groups 2 and 3, groups 2 and 4 (0.96), and groups 3 and 4 (all  $P < 0.001$ ), but not between groups 1 and 4 ( $P = 0.273$ ). The Sup/Inf ratio of LCD differed only between groups 2 and 3 ( $P = 0.002$ ).

**Conclusions:** Eyes with POAG showed regional differences in LC morphology, corresponding with the location of RNFL defects. The regional variations in LCCI suggest that LC morphology in POAG would be better assessed on a regional basis than by a global index. *Ophthalmology* 2019;■:1–10 © 2019 by the American Academy of Ophthalmology



Supplementary videos available online at [www.aajournal.org](http://www.aajournal.org).

Glaucoma is characterized by the loss of retinal ganglion cells and their axons, resulting in corresponding visual field (VF) defects. According to the mechanical theory of glaucoma, posterior lamina cribrosa (LC) deformation is regarded as playing a central role in the development of glaucomatous optic neuropathy.<sup>1</sup> The posterior deformation and associated compression of the LC are thought to promote axonal or retinal ganglion cell damage through diverse mechanisms, including a blockade of axonal transport and tissue remodeling by reactive astrocytes.<sup>2-5</sup> Furthermore, compression of the LC may affect the diffusion of nutrients from the capillaries within the laminar beams to the adjacent axons, thereby further compromising the axons.<sup>6</sup>

Despite the importance of LC deformation, little is known about the relationship between glaucomatous axonal damage and LC deformation. For example, whether the LC deformation is a prerequisite for the development of glaucomatous axonal damage and what degree of LC deformation is required for the development of axonal damage are unclear. In addition, regional variations in LC

deformation and their topographic relationship with axonal damage remain to be determined.

Eyes with early- to moderate-stage glaucoma often experience glaucomatous defects in only 1 hemifield. Because stress induced by increased intraocular pressure (IOP) is globally applied to the optic nerve head (ONH) within an eye, this phenomenon is intriguing. Previous studies have suggested a regional variability in connective tissue support of the axons (i.e., larger pores and thinner LC beams).<sup>7-9</sup> This variability may lead to differences in the vulnerability of areas of the LC to IOP-induced stress, resulting in a regional variability of LC deformation. That is, deformation may be greater in regions containing less dense connective tissue, resulting in greater damage to the corresponding region of optic disc.

From this perspective, determining the topographic relationship between LC morphology and damage to the retinal nerve fiber layer (RNFL) may increase understanding of the importance of LC deformation in the development of glaucomatous axonal damage. In addition, such knowledge would provide a platform to develop a method to best assess

LC morphology. The current study investigated the regional patterns of LC morphology in eyes with hemifield RNFL defects in a Korean population.

## Methods

This investigation was based on the Investigating Glaucoma Progression Study,<sup>10,11</sup> an ongoing prospective investigation of glaucoma and healthy subjects at the Seoul National University Bundang Hospital Glaucoma Clinic. All subjects met the eligibility criteria of the Investigating Glaucoma Progression Study and provided written informed consent to participate. This study was approved by the Seoul National University Bundang Hospital Institutional Review Board and conformed to the Declaration of Helsinki.

## Participants

Before the study, each patient underwent a complete ophthalmic examination, including assessments of visual acuity, refraction, slit-lamp biomicroscopy, gonioscopy, Goldmann applanation tonometry, and dilated stereoscopic examination of the optic disc, as well as measurements of corneal curvature (KR-1800; Topcon, Tokyo, Japan), central corneal thickness (Orbscan II; Bausch & Lomb Surgical, Rochester, NY), and axial length (AXL) (IOL-Master version 5; Carl Zeiss Meditec, Dublin, CA). All subjects were also assessed by stereo disc photography, red-free fundus photography (Kowa VX-10; Kowa Medicals, Torrance, CA), spectral-domain OCT (SD OCT, Spectralis OCT; Heidelberg Engineering, Heidelberg, Germany), and standard automated perimetry (Humphrey Field Analyzer II 750 and 24-2 Swedish interactive threshold algorithm; Carl Zeiss Meditec).

Subjects were included if they had a best-corrected visual acuity of at least 20/40, a spherical refraction of  $-8.0$  to  $+3.0$  diopters, and a cylinder correction within  $\pm 3.0$  diopters. Primary open-angle glaucoma (POAG) was defined as the presence of glaucomatous optic nerve damage (i.e., neuroretinal rim thinning/notching or splinter hemorrhage and the presence of RNFL defect in the corresponding region) and associated VF defects without ocular diseases or conditions that may elevate IOP. The RNFL defects identified by red-free photographs were confirmed by SD OCT circumpapillary RNFL thickness. A glaucomatous VF change was defined as (1) a change outside the normal limit on the glaucoma hemifield test; (2) 3 abnormal points with a  $<5\%$  probability of being normal or 1 point with a  $<1\%$  probability of being normal by pattern deviation; or (3) a pattern standard deviation  $<5\%$  on 2 consecutive reliable tests. A VF measurement was considered reliable when both false-positive and false-negative rates were  $<25\%$  and fixation losses were  $<20\%$ .

Healthy subjects had an IOP  $\leq 21$  mmHg with no history of increased IOP, an absence of glaucomatous disc appearance, no visible RNFL defect on red-free photography, and a normal VF. Absence of a glaucomatous disc appearance was defined as an intact neuroretinal rim without peripapillary hemorrhages, notches, or localized pallor. A normal VF was defined as the absence of glaucomatous VF defects and neurologic field defects.

Subjects with a history of intraocular surgery except uneventful cataract surgery or coexisting retinal (e.g., diabetic retinopathy, retinal vessel occlusion, or retinoschisis) or neurologic (e.g., pituitary tumor) diseases that could affect the VF were excluded from this study, as were patients with secondary (e.g., uveitic) glaucoma that could increase IOP. Eyes were also excluded when a good-quality image (i.e., quality score  $> 15$ ) could not be obtained in more than 5 sections of enhanced depth imaging (EDI) SD OCT disc scans (when the quality score does not reach 15, the image-acquisition process automatically stopped, and the image of

the respective sections is not obtained). Also excluded were eyes with a tilt ratio  $>1.3$  between the longest and shortest diameters of the optic disc<sup>12,13</sup> or torsion of the optic disc, defined as a torsion angle, calculated as the deviation of the long axis of the optic disc from the vertical meridian  $>15^\circ$ .<sup>13,14</sup>

Subjects were divided into 4 groups. Group 1 consisted of healthy subjects, and groups 2 to 4 consisted of naïve POAG patients showing superior RNFL defects with corresponding inferior hemi VF defects (group 2), inferior RNFL defects with corresponding superior hemi VF defects (group 3), and both superior and inferior RNFL defects with corresponding inferior and superior VF defects (group 4). To be included in groups 2 and 3, patients should have both RNFL defects and corresponding glaucomatous VF damage that were confined to a single hemifield. There should be no RNFL defect or abnormal visual field on the opposite hemifield in these groups. Subjects in the 4 groups were 1:1:1:1 by age, sex, and AXL.

## Enhanced Depth Imaging OCT of Optic Nerve Head

The optic nerve was imaged using the EDI technique of the Spectralis OCT system, a technique originally developed to visualize the full thickness of the choroid.<sup>15</sup> This technique yields images with a stronger signal and better image contrast in the deep ONH tissue than the conventional imaging technique.<sup>16</sup> Patients were imaged through undilated pupils using a rectangle subtending  $10^\circ \times 15^\circ$  of the optic disc. This rectangle was scanned with approximately 75 B-scan section images separated by 30 to 34  $\mu\text{m}$ , with the scan line distance determined automatically by the machine. Approximately 42 SD OCT frames were averaged for each section. This protocol provided the best trade-off between image quality and patient cooperation.<sup>16</sup> Potential magnification errors were avoided by entering the corneal curvature of each eye into the Spectralis OCT system before scanning.

To enhance the visibility of the anterior LC surface, all disc scan images were postprocessed using adaptive compensation,<sup>17-19</sup> and measurements were performed using a manual caliper tool in Amira software (version 5.2.2, Visage Imaging, Berlin, Germany) by 2 experienced observers (J.A.K. and E.J.L.) who were masked to subjects' clinical information. The mean of measurements by the 2 observers were used for analysis. The LC parameters on horizontal B-scan images were measured at 7 locations equidistant across the vertical optic disc diameter. Disc margin was defined as Bruch's membrane opening (BMO) visible in the B-scan images. These 7 B-scan lines were defined as planes 1 to 7 (top to bottom in Fig 1), with planes 2 and 6 corresponding approximately to the mid-periphery, and plane 4 to the mid-horizontal plane.

## Measurement of Lamina Cribrosa Curvature Index

To quantify the posterior bowing of LC on the SD OCT B-scan images, the LC curvature index (LCCI) was determined by assessing the inflection of a curve representing a section of the LC. The LCCI was measured as described previously.<sup>20,21</sup> In brief, the width ( $W$ ) of BMO was measured in each B-scan, followed by measurement of the LC curve depth (LCCD) (Fig 1). The BMO width was defined as the distance between the temporal and nasal termination points. Lines were drawn from each Bruch's membrane termination point perpendicular to the BMO reference line until they met the anterior LC surface. The line connecting the 2 points on the anterior LC surface was the reference line for measuring the LCCD, which was defined as the maximum LC depth (LCD) from the reference line (Fig 1). The LCCI was calculated as  $(\text{LCCD}/W) \times 100$ . Because the curvature was

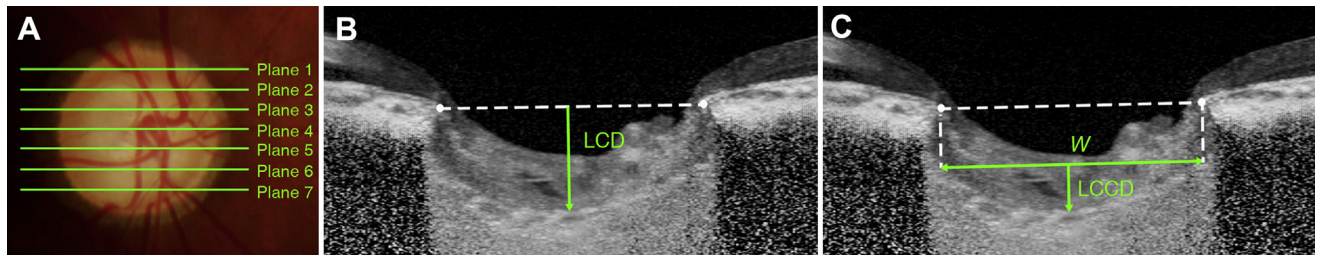


**Figure 1.** Measurements of the lamina cribrosa (LC) depth (LCD) and LC curvature index (LCCI). **A**, Disc photograph showing 7 horizontal green lines indicating the locations at which the measurements were performed. **B** and **C**, Enhanced depth imaging OCT B-scan images obtained in plane 6 in (**A**). **B**, The LCD was measured as the distance from the reference line connecting the 2 Bruch's membrane opening (BMO) points to the anterior surface of the LC. The LCD was measured at the maximally depressed point. **C**, The LCCI was measured by dividing the LC curve depth (LCCD) by the width of the anterior LC surface reference line ( $W$ ) and multiplying by 100.

normalized to LC width, it describes the shape of the LC independent of the actual size of the ONH. Specifically,  $(LCCD/W) \times 100$  is a simple normalized measure that represents the posterior bowing or curvature of the anterior LC surface within the BMO. Only the LC within the BMO was considered because the LC outside the BMO was often not clearly visible.

### Measurement of Lamina Cribrosa Depth

To determine the LCD, a line connecting the edges of the BMO was set as a reference plane (BMO reference line), and the LCD was measured perpendicular to the reference plane at the maximally depressed point (Fig 1).

### Comparison of Regional Lamina Cribrosa Morphology

The superior and inferior LCCIs were compared by dividing the superior mean (average of plane 1 to 3) LCCI by the inferior mean (average of planes 5 to 7) LCCI (superior-to-inferior [Sup/Inf] ratio), with a ratio  $>1$  indicating that the LC was more steeply curved in the superior than in the inferior ONH, and vice versa. The LCCIs of planes 1 and 7, 2 and 6, and 3 and 5 were also compared by dividing superior LCCI by inferior LCCI (plane 1/7, 2/6, and 3/5 ratio, respectively). Superior and inferior LCD were compared similarly.

### Statistical Analysis

The interobserver agreement for measuring LCCI and LCD was evaluated by calculating intraclass correlation coefficients. Differences in continuous variables among groups were compared by analysis of variance with the post hoc Tukey test, whereas categorical variables were compared using the Kruskal–Wallis test, with raw data subjected to Bonferroni correction based on the number of comparisons in each analysis. Linear regression analyses were performed to assess the associations between various clinical factors and LC parameters. Except where indicated otherwise, the data are presented as mean  $\pm$  standard deviation, and the cutoff for statistical significance was set at  $P < 0.05$ . All statistical analyses were performed using the Statistical Package for the Social Sciences software (version 22.0, SPSS, Chicago, IL).

## Results

### Demographic and Clinical Characteristics

This cross-sectional study initially involved 234 patients with POAG and 65 healthy subjects; of these, 54 and 13, respectively, were

excluded because of the presence of a tilted disc. Twelve subjects were further excluded because of poor image quality, preventing the clear visualization of the anterior LC surface in at least 2 of the 7 EDI-OCT B-scan images. After matching for age, sex, and AXL, each group consisted of 39 eyes of 39 subjects (total, 156 eyes).

Table 1 summarizes the demographic and clinical characteristics of the included subjects. The IOP at the time of EDI-OCT was lower in group 1 than in the other 3 groups ( $P = 0.002$ ). There were no significant differences in age, sex, spherical equivalent, central corneal thickness, AXL, blood pressure, migraine, and self-reported cold extremities.

### Differences in Lamina Cribrosa Curvature Index and Lamina Cribrosa Depth between Glaucomatous and Healthy Eyes

Measurements of LCCI and LCD showed excellent intraobserver reproducibility, with intraclass correlation coefficients for LCCI of 0.979 (range, 0.970–0.986) and for LCD of 0.969 (range, 0.948–0.982).

Figure 2 shows the measured LCCI and LCD values in each group. Compared with healthy eyes (group 1), LCCI was larger in the superior and middle planes (planes 1–5) in group 2 (all  $P \leq 0.003$ ), the inferior and middle planes (planes 4–7) in group 3 (all  $P \leq 0.001$ ), and all planes in group 4 (all  $P < 0.001$ , Table 2).

The LCD in all planes did not differ significantly in groups 1 and 2. Compared with group 1, LCD was significantly larger in the inferior planes (planes 5–7) in group 3 (all  $P \leq 0.003$ ) and in all planes in group 4 (all  $P \leq 0.005$ , Table 2).

### Regional Variations of Lamina Cribrosa Curvature Index

Mean Sup/Inf ratios in groups 1 to 4 were  $1.03 \pm 0.15$ ,  $1.20 \pm 0.21$ ,  $0.79 \pm 0.15$ , and  $0.96 \pm 0.19$ , respectively (Table 3, Fig 3). The Sup/Inf ratio was significantly higher in group 2 than in group 1 ( $P < 0.001$ ) and was significantly lower in group 3 than in group 1 ( $P < 0.001$ ). However, this ratio did not differ significantly between groups 1 and 4.

Similar results were also observed for the plane 1/7 and plane 2/6 ratios, except that the latter did not differ significantly between groups 1 and 2. In contrast, plane 3/5 ratios differed significantly only between groups 1 and 3, groups 2 and 3, and groups 2 and 4 (all  $P \leq 0.003$ ). Figure 4 shows representative eyes with superior and inferior RNFL defects.

### Regional Comparisons of Lamina Cribrosa Depth

The Sup/Inf, plane 2/6, and plane 3/5 ratios differed significantly between groups 2 and 3 (all  $P \leq 0.004$ ). The plane 3/5 ratio also

Table 1. Demographic Characteristics of the Study Subjects

Variables	Group 1 (n=39)	Group 2 (n=39)	Group 3 (n=39)	Group 4 (n=39)	P Value	Post Hoc Analysis
Age, yrs	55.9±10.8	56.6±10.9	56.1±11.0	56.1±10.8	0.994*	
Female, no. (%)	26 (66.7)	26 (66.7)	26 (66.7)	26 (66.7)	1.000 <sup>†</sup>	
Spherical equivalent, D	-0.02±1.45	-0.46±1.66	-0.34±1.52	-0.19±1.66	0.641*	
Axial length, mm	23.9±0.9	24.0±1.0	23.8±0.9	23.8±0.9	0.822*	
Central corneal thickness, $\mu$ m	554.7±42.7	550.1±36.6	548.1±34.2	543.6±33.3	0.608*	
Intraocular pressure, mmHg	12.4±2.8	14.9±4.8	14.8±2.7	15.3±3.9	<b>0.002*</b>	1<2=3=4
Self-reported history of diabetes, no. (%)	4 (10.3)	4 (10.3)	3 (7.7)	2 (5.1)	0.821 <sup>†</sup>	
Self-reported history of hypertension, no. (%)	6 (15.4)	14 (35.9)	16 (41.0)	13 (33.3)	0.082 <sup>†</sup>	
Glaucoma family history, no. (%)	5 (15.4)	2 (5.1)	1 (2.6)	5 (15.4)	0.235 <sup>†</sup>	
Migraine, no. (%)	8 (20.5)	8 (20.5)	7 (17.9)	2 (5.1)	0.213 <sup>†</sup>	
Cold extremities, no. (%)	11 (28.2)	10 (25.6)	6 (15.4)	8 (20.5)	0.551 <sup>†</sup>	
Systolic blood pressure, mmHg	125.3±13.6	124.6±14.0	128.3±16.8	122.6±10.3	0.333*	
Diastolic blood pressure, mmHg	71.8±7.3	72.5±9.5	75.5±7.8	75.8±7.6	0.064*	
Mean arterial pressure, mmHg	89.6±8.4	89.9±10.0	93.1±9.7	91.4±7.3	0.296*	
Mean ocular perfusion pressure, mmHg	51.5±5.0	50.0±7.3	52.3±6.8	50.7±5.4	0.400*	

D = diopters; POAG = primary open-angle glaucoma; RNFL = retinal nerve fiber layer.

Data are mean  $\pm$  standard deviation values, with statistically significant P values (<0.05) in boldface. Statistical significance tested by \*analysis of variance and <sup>†</sup>Kruskal–Wallis test.

Group 1 = healthy; group 2 = naïve POAG with superior RNFL defect; group 3 = naïve POAG with inferior RNFL defect; group 4 = naïve POAG with both RNFL defects.

differed significantly between groups 3 and 4, but there were no significant differences in other comparisons of regional LCD.

### Factors Associated with Sup/Inf Ratios of Lamina Cribrosa Curvature Index and Lamina Cribrosa Depth

Linear regression analysis showed no covariates associated with the Sup/Inf and planes 1/7, 2/6, and 3/5 ratios (Table 4).

### Discussion

The present study demonstrated regional differences in LC curvature in POAG eyes differing in their locations of RNFL/VF defects. The LC curvature was greater at the planes corresponding to the location of the RNFL defect. To our knowledge, there has been no study in the literature correlating the location of the RNFL defect and regional variations in LC morphology.

Because LC morphology is highly variable on vertical and radial scans, LCCI and LCD in the present study were

measured using horizontal B-scan images. A horizontal ridge at or near the mid-horizontal ONH<sup>22</sup> results in the anterior LC surface having a W-shaped configuration in vertical and oblique scans (i.e., the LC would have at least 2 separate curvatures; Video 1, available at [www.aojournal.org](http://www.aojournal.org)). Therefore, analysis of the LC configuration using vertical or oblique scans would be complicated.<sup>21</sup> In contrast, the LC has a relatively regular configuration in the horizontal plane, with a flat or U-shaped appearance with different regional steepness, allowing the measurement of LCCI (Video 2, available at [www.aojournal.org](http://www.aojournal.org)).<sup>21</sup>

Regional differences in LC morphology were analyzed by measuring the Sup/Inf ratios of LC indexes as well as their absolute values, thereby compensating for innate interindividual variations in LCD and LCCI. Subjects with a higher initial LCCI or LCD would have higher subsequent LCCI or LCD despite a lower degree of posterior LC deformation. Thus, only comparing absolute values may lead to erroneous conclusions.

Plane 4 was considered as the mid-horizontal plane in all patients. This idea was based on the assumption that the

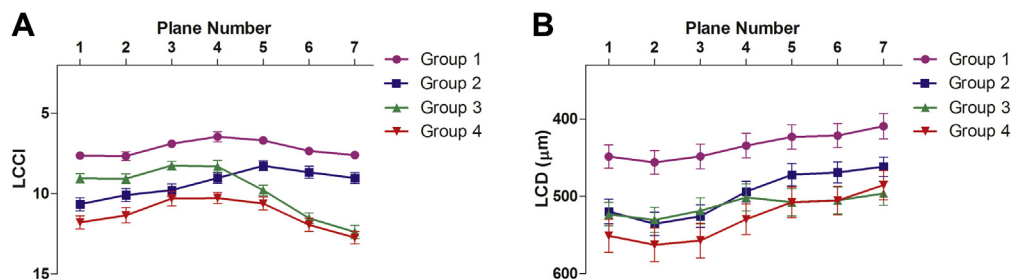


Figure 2. Graph showing variations in lamina cribrosa curvature index (LCCI) and lamina cribrosa depth (LCD) in the different planes and groups. Error bars represent standard error of the mean. Group 1 = healthy; group 2 = naïve primary open-angle glaucoma (POAG) with superior retinal nerve fiber layer (RNFL) defect; group 3 = naïve POAG with inferior RNFL defect; group 4 = naïve POAG with both RNFL defects.

Table 2. Comparison of Lamina Cribrosa Curvature Index and Lamina Cribrosa Depth between Healthy and Primary Open-Angle Glaucoma Eyes

LCCI								
Plane Number	Group 1: Healthy (n=39)	Group 2: Superior Hemifield Defect (n=39)	Group 3: Inferior Hemifield Defect (n=39)	Group 4: Both Hemifield Defect (n=39)	P Value	Post Hoc Analysis		
						Group 1 vs. Group 2	Group 1 vs. Group 3	Group 1 vs. Group 4
1	7.64±1.26	10.68±2.54	9.05±1.83	11.80±2.59	<b>&lt;0.001</b>	<b>&lt;0.001</b>	0.020	<b>&lt;0.001</b>
2	7.68±1.74	10.09±2.57	9.08±1.88	11.36±2.93	<b>&lt;0.001</b>	<b>&lt;0.001</b>	0.043	<b>&lt;0.001</b>
3	6.90±1.47	9.79±2.37	8.26±1.65	10.32±2.80	<b>&lt;0.001</b>	<b>&lt;0.001</b>	0.030	<b>&lt;0.001</b>
4	6.47±1.96	9.04±2.03	8.32±2.24	10.29±2.21	<b>&lt;0.001</b>	<b>&lt;0.001</b>	0.001	<b>&lt;0.001</b>
5	6.69±1.35	8.28±1.89	9.80±1.98	10.63±2.56	<b>&lt;0.001</b>	<b>0.003</b>	<b>&lt;0.001</b>	<b>&lt;0.001</b>
6	7.35±1.17	8.68±2.29	11.54±2.04	11.96±2.61	<b>&lt;0.001</b>	0.029	<b>&lt;0.001</b>	<b>&lt;0.001</b>
7	7.60±1.29	9.03±2.16	12.39±2.55	12.76±2.43	<b>&lt;0.001</b>	0.021	<b>&lt;0.001</b>	<b>&lt;0.001</b>

LCD								
Plane Number	Group 1: Healthy (n=39)	Group 2: Superior Hemifield Defect (n=39)	Group 3: Inferior Hemifield Defect (n=39)	Group 4: Both Hemifield Defect (n=39)	P Value	Post hoc analysis		
						Group 1 vs. Group 2	Group 1 vs. Group 3	Group 1 vs. Group 4
1	448.69±93.66	519.85±99.59	523.31±95.61	551.33±133.41	<b>&lt;0.001</b>	0.020	0.013	<b>&lt;0.001</b>
2	456.08±95.32	535.85±93.65	530.56±101.79	562.92±135.71	<b>&lt;0.001</b>	0.007	0.014	<b>&lt;0.001</b>
3	448.54±98.85	525.82±90.54	518.92±106.25	557.31±139.29	<b>&lt;0.001</b>	0.012	0.028	<b>&lt;0.001</b>
4	434.41±99.25	494.03±83.06	501.54±109.90	529.87±124.30	<b>0.001</b>	0.064	0.028	<b>0.001</b>
5	423.33±98.90	472.28±89.68	507.92±110.60	507.85±123.05	<b>0.001</b>	0.180	<b>0.003</b>	<b>0.003</b>
6	421.54±98.47	469.08±84.89	505.36±107.69	505.54±115.45	<b>0.001</b>	0.174	<b>0.002</b>	<b>0.002</b>
7	409.26±102.04	461.79±78.34	496.31±96.76	485.67±117.35	<b>0.001</b>	0.096	<b>0.001</b>	<b>0.005</b>

LCCI = lamina cribrosa curvature index; LCD = lamina cribrosa depth; POAG = primary open-angle glaucoma; RNFL = retinal nerve fiber layer. Data are mean ± standard deviation values, with statistically significant *P* values in boldface. Bonferroni correction was applied to raw data for measurements in the 7 locations. Values that were significant after Bonferroni correction ( $P < 0.007; 0.05/7$ ) are shown in bold. Statistical significance tested by analysis of variance.

Group 1 = healthy; group 2 = naïve POAG with superior RNFL defect; group 3 = naïve POAG with inferior RNFL defect; group 4 = naïve POAG with both RNFL defects.

ONH is symmetric (i.e., the horizontal ridge is located at the geometric mid-horizon). However, this may not be the case in all patients. Such variation may have affected the result. The more obvious difference of LCCI between plane 1 and 7 (planes farthest from the mid-horizontal plane) than between plane 3 and 5 (planes closest to the mid-horizontal plane) may be partly attributed to this matter.

The patient classification was based on the presence of an RNFL defect and corresponding VF defect in 1 hemifield or both hemifields. In this process, patients who had an RNFL defect without corresponding VF damage (i.e., preperimetric RNFL defect) in any hemifield were not included in the analysis. However, it is possible that some patients included in group 2 or 3 might have started early glaucomatous change in the opposite hemifield that was not detected by red-free photography or OCT. In other words, the glaucomatous damage might have not been completely limited to 1 hemifield in some patients in group 2 and 3. This should be considered when interpreting the result of the current study.

Damage to the optic nerve in glaucoma occurs preferentially in the superior or inferior region. This tendency toward regional glaucomatous damage may result from regional variations in the LC (i.e., larger pores and thinner LC beams in the superior and inferior peripheral regions than in the central region).<sup>7-9</sup> Our findings are in line with this concept and provide insight into the relationship between LC density and axonal damage.

This study demonstrated that the LCCI was greater at the location of axonal damage. Although regional LCCI variation may be innate, larger LCCI can be derived from acquired bowing induced by translaminar pressure difference. This idea is supported by the finding that LCCI is larger in eyes with higher IOP<sup>20</sup> and varies depending on the level of IOP within an individual.<sup>23</sup> The LCCI can indicate the position of the LC due to native IOP at the moment of the scan or can change over time with age or due to glaucomatous connective tissue remodeling or both. Assuming that large LCCI reflects greater LC bowing, our finding may suggest that the regional variability of LC exists in terms of susceptibility to translaminar pressure difference. The degree of regional LC deformation is probably affected by the material property of the LC at that region.<sup>24</sup> That is, posterior LC deformation would occur first in the region of lower density. Taken together, these findings suggest the possibility that posterior LC deformation first occurs at the location of least dense LC, leading to subsequent development of glaucomatous axonal damage at the corresponding location.

Evaluation of the LC may have clinical value. Studies have shown that assessment of LC morphology may be useful in the differential diagnosis of glaucoma from other optic neuropathies<sup>25</sup> and predict disease outcome.<sup>26,27</sup> The current study demonstrated that LC curvature varied depending on horizontal planes within single ONH, being

Table 3. Comparison of Superior/Inferior Ratio of Lamina Cribrosa Curvature Index and Lamina Cribrosa Depth between Healthy and Primary Open-Angle Glaucoma Eyes

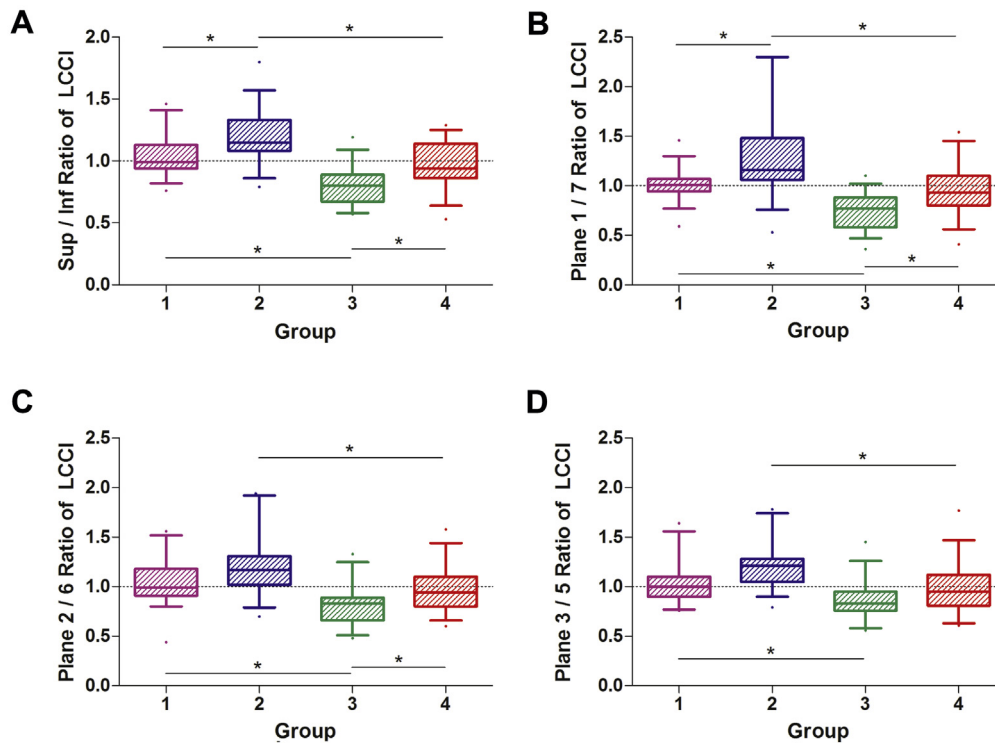
LCCI											
Plane Ratio	Group 1: Healthy (n=39)	Group 2: Superior Hemifield Defect (n=39)	Group 3: Inferior Hemifield Defect (n=39)	Group 4: Both Hemifield Defect (n=39)	P Value	Post Hoc Analysis					
						Group 1 vs. Group 2	Group 1 vs. Group 3	Group 1 vs. Group 4	Group 2 vs. Group 3	Group 2 vs. Group 4	Group 3 vs. Group 4
Superior Mean/Inferior Mean Ratio	1.03±0.15	1.20±0.21	0.79±0.15	0.96±0.19	<b>&lt;0.001</b>	<b>&lt;0.001</b>	<b>&lt;0.001</b>	0.273	<b>&lt;0.001</b>	<b>&lt;0.001</b>	<b>&lt;0.001</b>
Plane 1/7 Ratio	1.02±0.16	1.26±0.37	0.75±0.18	0.96±0.26	<b>&lt;0.001</b>	<b>&lt;0.001</b>	<b>&lt;0.001</b>	0.687	<b>&lt;0.001</b>	<b>&lt;0.001</b>	<b>0.003</b>
Plane 2/6 Ratio	1.05±0.23	1.20±0.27	0.80±0.19	0.97±0.23	<b>&lt;0.001</b>	0.029	<b>&lt;0.001</b>	0.421	<b>&lt;0.001</b>	<b>&lt;0.001</b>	<b>0.008</b>
Plane 3/5 Ratio	1.06±0.32	1.20±0.22	0.86±0.19	0.99±0.26	<b>&lt;0.001</b>	0.085	<b>0.002</b>	0.623	<b>&lt;0.001</b>	<b>0.003</b>	0.084

LCD											
Plane Ratio	Group 1: Healthy (n=39)	Group 2: Superior Hemifield Defect (n=39)	Group 3: Inferior Hemifield Defect (n=39)	Group 4: Both Hemifield Defect (n=39)	P Value	Post Hoc Analysis					
						Group 1 vs. Group 2	Group 1 vs. Group 3	Group 1 vs. Group 4	Group 2 vs. Group 3	Group 2 vs. Group 4	Group 3 vs. Group 4
Superior Mean/Inferior Mean Ratio	1.09±0.11	1.13±0.09	1.05±0.10	1.12±0.10	<b>0.002</b>	0.232	0.317	0.625	<b>0.002</b>	0.898	0.021
Plane 1/7 Ratio	1.12±0.17	1.13±0.15	1.07±0.14	1.14±0.13	0.127						
Plane 2/6 Ratio	1.09±0.12	1.15±0.12	1.06±0.12	1.11±0.11	<b>0.008</b>	0.128	0.613	0.853	<b>0.004</b>	0.503	0.183
Plane 3/5 Ratio	1.06±0.09	1.12±0.12	1.03±0.08	1.10±0.10	<b>&lt;0.001</b>	0.044	0.349	0.425	<b>&lt;0.001</b>	0.675	<b>0.009</b>

LCCI = lamina cribrosa curvature index; LCD = lamina cribrosa depth.

Data are mean ± standard deviation values, with statistically significant P values in boldface. Values that were significant after Bonferroni correction ( $P < 0.013$ ;  $0.05/4$ ) are shown in bold. Statistical significance tested by analysis of variance.



**Figure 3.** Graph showing the (A) superior-to-inferior (Sup/Inf) ratio, (B) plane 1/7, (C) plane 2/6, and (D) plane 3/5 ratios of the lamina cribrosa curvature index (LCCI). The box plots show the median, interquartile range, 95th percentile, and extreme values. There was no significant difference in Sup/Inf ratio between groups 1 and 4. Group 2 had a larger and group 3 had a smaller Sup/Inf ratio than groups 1 and 4. The between-group differences in LCCI ratios corresponded with the location of retinal nerve fiber layer (RNFL) defects. Group 1 = healthy; group 2 = naïve primary open-angle glaucoma (POAG) with superior RNFL defect; group 3 = naïve POAG with inferior RNFL defect; group 4 = naïve POAG with both RNFL defects. \*Bonferroni-corrected  $P < 0.013$ , analysis of variance.

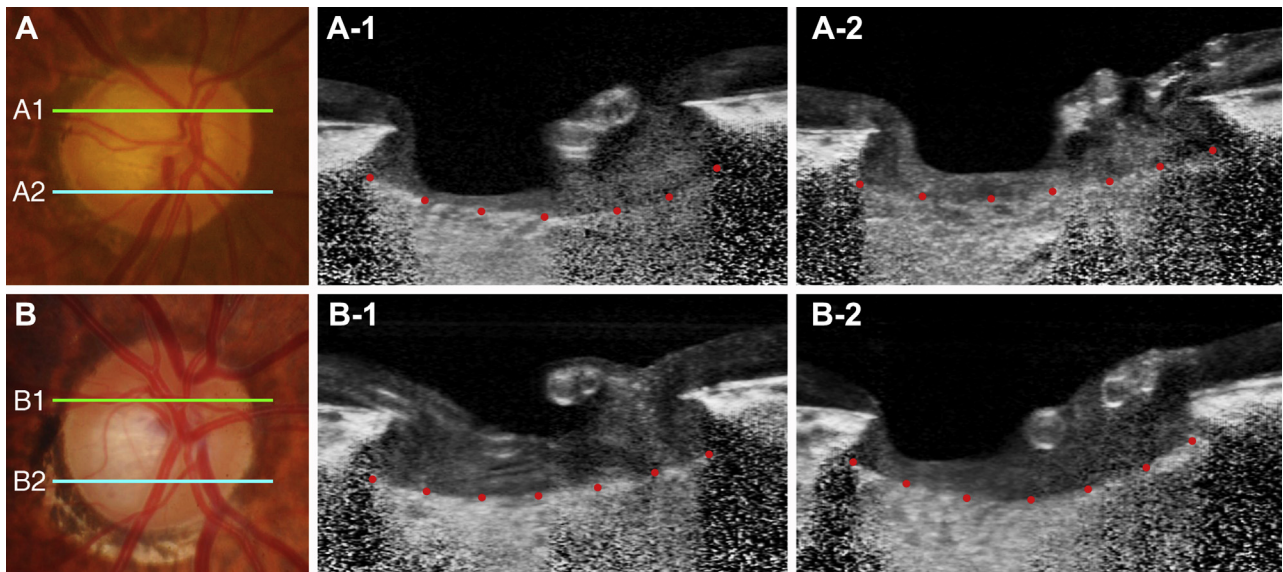


**Figure 4.** Representative eyes with superior (A) and inferior (B) rim thinning from a 69-year-old man and a 72-year-old man, respectively. A-1 and B-1, Superior B-scan images at plane 2, indicated by the green line in the optic disc photographs. A-2 and B-2, Inferior B-scan images at plane 6, indicated by the blue line in the optic disc photographs. Note that the lamina cribrosa (LC) curvature was noticeably steeper at the hemisphere with rim thinning in both eyes. The lamina cribrosa curvature index (LCCI) in panels A1, A2, B1, and B2 were 11.75, 8.02, 8.39, and 13.32, respectively.

Table 4. Factors Associated with the Mean Superior/Inferior Lamina Cribrosa Curvature Index and Lamina Cribrosa Depth Ratio

Variables	Superior/Inferior LCCI Ratio				Superior/Inferior LCD Ratio			
	Healthy		POAG		Healthy		POAG	
	$\beta$	P	$\beta$	P	$\beta$	P	$\beta$	P
Age, per 1 yr older	0.001	0.565	0.001	0.760	0.001	0.975	0.001	0.186
Male gender	0.059	0.254	0.028	0.568	-0.003	0.945	0.008	0.676
SE, per 1 D larger	-0.004	0.828	-0.010	0.509	-0.011	0.387	0.008	0.172
AXL, per 1 mm larger	0.039	0.162	0.002	0.939	-0.006	0.753	-0.008	0.467
CCT, per 1 $\mu$ m larger	0.000	0.822	0.001	0.071	0.001	0.902	0.000	0.223
Baseline IOP, per 1 mmHg higher	0.011	0.189	0.006	0.316	0.006	0.359	-0.002	0.499
Self-reported diabetes	0.032	0.695	0.034	0.690	-0.034	0.559	0.009	0.793
Self-reported hypertension	0.023	0.735	0.010	0.830	-0.054	0.262	0.019	0.332
Family history of glaucoma	-0.113	0.115	0.028	0.758	0.026	0.627	0.005	0.901
Migraine	-0.034	0.570	-0.043	0.508	-0.037	0.398	-0.038	0.161
Cold extremities	-0.072	0.178	0.018	0.746	0.030	0.440	-0.003	0.914
Systolic blood pressure, per 1 mmHg higher	-0.001	0.639	0.000	0.847	-0.002	0.229	-0.001	0.173
Diastolic blood pressure, per 1 mmHg higher	0.003	0.381	-0.003	0.267	-0.003	0.281	-0.002	0.065
Location of RNFL defect	N/A	N/A	-0.120	<b>&lt;0.001</b>	N/A	N/A	-0.008	0.499

AXL = axial length; CCT = central corneal thickness; D = diopters; IOP = intraocular pressure; LCCI = lamina cribrosa curvature index; LCD = lamina cribrosa depth; N/A = not available; POAG = primary open-angle glaucoma; RNFL = retinal nerve fiber layer; SE = spherical equivalent.

prominent in the region corresponding to RNFL damage. This finding suggests that it may be better to evaluate LC curvature on a regional rather than a global basis, because global evaluation may miss small degrees of localized LC deformation.

The LCD also showed intergroup differences. However, there were no significant differences between groups 1 and 2 at the superior location. The LCD is larger in the superior plane than in the inferior plane in both healthy and glaucomatous eyes.<sup>28-30</sup> Therefore, the same degree of LC deepening would result in smaller proportional changes in the superior than in the inferior region and may explain the lack of significant difference in the superior planes.

The LCCI ratios comparing superior and inferior regions showed differences between all pairs of groups except groups 1 and 4. However, LCD ratios differed only for groups 2 and 3, likely because of the opposite locations of their RNFL defects. This finding is likely associated with the limited ability of LCD to characterize glaucomatous LC morphology as demonstrated previously.<sup>20,21</sup> Because the LCD was measured from the BMO, it should be influenced by the choroidal thickness, which varies among individuals.<sup>31</sup> The LC is a sieve-like perforation in the posterior part of the sclera and is sustained by load-bearing connective tissues of the peripapillary sclera. Thus, including the choroidal thickness in the LCD would lead to a biased assessment of LC morphology.<sup>20,32</sup>

### Study Limitations

This study had several limitations. First, an LC surface reference line from the LC insertion points may have allowed a more precise quantification of the LC curve. However, in measuring the LC curve, the present study included only the LC within the BMO width, because the LC was often not visible outside this region. However, we previously demonstrated that the LCCI measured using the entire LC (i.e., between the LC insertions) was comparable

to that measured on the LC within the BMO in eyes with an LC visible up to the LC insertion.<sup>23</sup> Thus, the LC curve within the BMO is representative of the actual LC curve. Second, we referred to the bowed LC configuration as LC curvature; however, the curvature is a geometric entity that refers to the inverse of the radius of the arc of a circle best fitting the portion of the curve. Thus, LCCI should not be considered a parameter corresponding to an actual LC curvature, suggesting the need for further study to investigate the method of calculating the actual curvature of the LC.<sup>23</sup> Third, because eyes with a tilted or torped optic disc were excluded, our findings cannot be directly applied to eyes with these conditions. Fourth, LCCI was measured only in horizontal scans. As described previously, this was to avoid the complexity in the analysis of LCCI using the vertical scan. However, LCCI in vertical scan may provide additional information that may help assess the LC curvature more comprehensively. Finally, this study included only Korean patients, and so it is possible that the present findings cannot be extrapolated to other ethnic populations.

In conclusion, regional differences in LC morphology, which corresponded with the location of the RNFL defect, were observed in eyes with POAG. This finding is in accord with the concept that deformation of the LC is a principal event in the development of glaucomatous optic neuropathy. The regional variations of the LCCI suggested the need to assess LC morphology on a regional rather than a global basis in eyes with POAG.

### References

1. Quigley HA, Addicks EM, Green WR, Maumenee AE. Optic nerve damage in human glaucoma. II. The site of injury and susceptibility to damage. *Arch Ophthalmol.* 1981;99:635-649.

2. Anderson DR, Hendrickson A. Effect of intraocular pressure on rapid axoplasmic transport in monkey optic nerve. *Invest Ophthalmol*. 1974;13:771–783.
3. Minckler DS, Bunt AH, Johanson GW. Orthograde and retrograde axoplasmic transport during acute ocular hypertension in the monkey. *Invest Ophthalmol Vis Sci*. 1977;16:426–441.
4. Minckler DS, Tso MO. A light microscopic, autoradiographic study of axoplasmic transport in the normal rhesus optic nerve head. *Am J Ophthalmol*. 1976;82:1–15.
5. Hernandez MR. The optic nerve head in glaucoma: role of astrocytes in tissue remodeling. *Prog Retin Eye Res*. 2000;19:297–321.
6. Burgoyne CF, Downs JC, Bellezza AJ, et al. The optic nerve head as a biomechanical structure: a new paradigm for understanding the role of IOP-related stress and strain in the pathophysiology of glaucomatous optic nerve head damage. *Prog Retin Eye Res*. 2005;24:39–73.
7. Quigley HA, Addicks EM. Regional differences in the structure of the lamina cribrosa and their relation to glaucomatous optic nerve damage. *Arch Ophthalmol*. 1981;99:137–143.
8. Quigley HA, Hohman RM, Addicks EM, et al. Morphologic changes in the lamina cribrosa correlated with neural loss in open-angle glaucoma. *Am J Ophthalmol*. 1983;95:673–691.
9. Jonas JB, Mardin CY, Schlotzer-Schrehardt U, Naumann GO. Morphometry of the human lamina cribrosa surface. *Invest Ophthalmol Vis Sci*. 1991;32:401–405.
10. Kim YW, Lee EJ, Kim TW, et al. Microstructure of beta-zone parapapillary atrophy and rate of retinal nerve fiber layer thinning in primary open-angle glaucoma. *Ophthalmology*. 2014;121:1341–1349.
11. Choi YJ, Lee EJ, Kim BH, Kim TW. Microstructure of the optic disc pit in open-angle glaucoma. *Ophthalmology*. 2014;121:2098–2106.e2092.
12. Jonas JB, Papastathopoulos KI. Optic disc shape in glaucoma. *Graefes Arch Clin Exp Ophthalmol*. 1996;234(Suppl 1):S167–S173.
13. Vongphanit J, Mitchell P, Wang JJ. Population prevalence of tilted optic disks and the relationship of this sign to refractive error. *Am J Ophthalmol*. 2002;133:679–685.
14. Samarawickrama C, Mitchell P, Tong L, et al. Myopia-related optic disc and retinal changes in adolescent children from Singapore. *Ophthalmology*. 2011;118:2050–2057.
15. Spaide RF, Koizumi H, Pozzoni MC. Enhanced depth imaging spectral-domain optical coherence tomography. *Am J Ophthalmol*. 2008;146:496–500.
16. Lee EJ, Kim TW, Weinreb RN, et al. Visualization of the lamina cribrosa using enhanced depth imaging spectral-domain optical coherence tomography. *Am J Ophthalmol*. 2011;152:87–95.e81.
17. Girard MJ, Tun TA, Husain R, et al. Lamina cribrosa visibility using optical coherence tomography: comparison of devices and effects of image enhancement techniques. *Invest Ophthalmol Vis Sci*. 2015;56:865–874.
18. Girard MJ, Strouthidis NG, Ethier CR, Mari JM. Shadow removal and contrast enhancement in optical coherence tomography images of the human optic nerve head. *Invest Ophthalmol Vis Sci*. 2011;52:7738–7748.
19. Mari JM, Strouthidis NG, Park SC, Girard MJ. Enhancement of lamina cribrosa visibility in optical coherence tomography images using adaptive compensation. *Invest Ophthalmol Vis Sci*. 2013;54:2238–2247.
20. Lee SH, Kim TW, Lee EJ, et al. Diagnostic power of lamina cribrosa depth and curvature in glaucoma. *Invest Ophthalmol Vis Sci*. 2017;58:755–762.
21. Lee EJ, Kim T-W, Kim H, et al. Comparison between lamina cribrosa depth and curvature as a predictor of progressive retinal nerve fiber layer thinning in primary open-angle glaucoma. *Ophthalmol Glaucoma*. 2018;1:44–51.
22. Park SC, Kiumehr S, Teng CC, et al. Horizontal central ridge of the lamina cribrosa and regional differences in laminar insertion in healthy subjects. *Invest Ophthalmol Vis Sci*. 2012;53:1610–1616.
23. Lee SH, Yu DA, Kim TW, et al. Reduction of the lamina cribrosa curvature after trabeculectomy in glaucoma. *Invest Ophthalmol Vis Sci*. 2016;57:5006–5014.
24. Quigley HA, Dorman-Pease ME, Brown AE. Quantitative study of collagen and elastin of the optic nerve head and sclera in human and experimental monkey glaucoma. *Curr Eye Res*. 1991;10:877–888.
25. Lee EJ, Choi YJ, Kim TW, Hwang JM. Comparison of the deep optic nerve head structure between normal-tension glaucoma and nonarteritic anterior ischemic optic neuropathy. *PLoS One*. 2016;11:e0150242.
26. Lee EJ, Kim TW, Kim M, Kim H. Influence of lamina cribrosa thickness and depth on the rate of progressive retinal nerve fiber layer thinning. *Ophthalmology*. 2015;122:721–729.
27. Lee EJ, Kim TW. Lamina cribrosa reversal after trabeculectomy and the rate of progressive retinal nerve fiber layer thinning. *Ophthalmology*. 2015;122:2234–2242.
28. Park SC, Brumm J, Furlanetto RL, et al. Lamina cribrosa depth in different stages of glaucoma. *Invest Ophthalmol Vis Sci*. 2015;56:2059–2064.
29. Seo JH, Kim TW, Weinreb RN. Lamina cribrosa depth in healthy eyes. *Invest Ophthalmol Vis Sci*. 2014;55:1241–1251.
30. Kim JA, Kim TW, Weinreb RN, et al. Lamina cribrosa morphology predicts progressive retinal nerve fiber layer loss in eyes with suspected glaucoma. *Sci Rep*. 2018;8:738.
31. Rhodes LA, Huisingh C, Johnstone J, et al. Peripapillary choroidal thickness variation with age and race in normal eyes. *Invest Ophthalmol Vis Sci*. 2015;56:1872–1879.
32. Vianna JR, Lanoe VR, Quach J, et al. Serial changes in lamina cribrosa depth and neuroretinal parameters in glaucoma: impact of choroidal thickness. *Ophthalmology*. 2017;124:1392–1402.

## Footnotes and Financial Disclosures

Originally received: August 20, 2018.

Final revision: November 27, 2018.

Accepted: December 12, 2018.

Available online: ■■■■.

Manuscript no. 2018-1879.

<sup>1</sup> Department of Ophthalmology, Seoul National University College of Medicine, Seoul National University Bundang Hospital, Seongnam, Korea.

<sup>2</sup> Department of Biomedical Engineering, National University of Singapore, Singapore.

<sup>3</sup> Singapore Eye Research Institute, Singapore National Eye Centre, Singapore.

<sup>4</sup> GePaSud, Université de la Polynésie Française, Tahiti, French Polynesia.

Financial Disclosure(s):

The author(s) have no proprietary or commercial interest in any materials discussed in this article.

Supported by Seoul National University Bundang Hospital Research Fund (No. 02-2016-023). The funder had no role in the design or conduct of this research.

**HUMAN SUBJECTS:** Human subjects were included in this study. The human ethics committees at the Seoul National University Bundang Hospital approved the study. All research adhered to the tenets of the Declaration of Helsinki. All participants provided informed consent.

No animal subjects were used in this study.

Author Contributions:

Conception and design: Kim, Kim

Analysis and interpretation: Kim, Kim, Lee

Data collection: Kim, Kim, Lee, Girard, Mari

Obtained funding: T-W. Kim (Seoul National University Bundang Hospital, South Korea)

Overall responsibility: Kim, Kim

Abbreviations and Acronyms:

**AXL** = axial length; **BMO** = Bruch's membrane opening; **EDI** = enhanced depth imaging; **IOP** = intraocular pressure; **LC** = lamina cribrosa; **LCCD** = lamina cribrosa curve depth; **LCCI** = lamina cribrosa curvature index; **LCD** = lamina cribrosa depth; **ONH** = optic nerve head; **POAG** = primary open-angle glaucoma; **RNFL** = retinal nerve fiber layer; **SD OCT** = spectral domain OCT; **Sup/Inf** = superior-to-inferior; **VF** = visual field.

Correspondence:

Tae-Woo Kim, MD, Department of Ophthalmology, Seoul National University Bundang Hospital, Seoul National University College of Medicine 82, Gumi-ro, 173 Beon-gil, Bundang-gu, Seongnam, Gyeonggi-do 463-707, Korea. E-mail: [twkim7@snu.ac.kr](mailto:twkim7@snu.ac.kr).